JOURNAL OF FUEL CHEMISTRY AND TECHNOLOGY
Volume 41, Issue 2, February 2013
Online English edition of the Chinese language journal

Available online at www.sciencedirect.com
ScienceDirect

Cite this article as: J Fuel Chem Technol, 2013, 41(2), 235–242

RESEARCH PAPER

Oxygen release kinetics and mechanism study on Cu-, Co-, Mn-based oxygen carrier

MEI Dao-feng, ZHAO Hai-bo*, MA Zhao-jun, YANG Wei-jin, FANG Yan-fei, ZHENG Chu-guang

State Key Laboratory of Coal Combustion, Huazhong University of Science & Technology, Wuhan 430074, China

Abstract: Sol-gel derived $CuO/CuAl_2O_4$, $Co_3O_4/CoAl_2O_4$ and Mn_2O_3/Al_2O_3 oxygen carriers were studied in a fluidized bed reactor under CO_2 atmosphere, where the oxygen release characteristics under different temperatures were focused. The mechanism function and kinetics parameters in the oxygen release were obtained from the experimental data. In the process of oxygen release, the phases of CuO and $CuAl_2O_4$ performing as active components decompose to Cu_2O and $CuAlO_2$ with O_2 generation. While, only Co_3O_4 and Mn_2O_3 can release oxygen in $Co_3O_4/CoAl_2O_4$ and Mn_2O_3/Al_2O_3 oxygen carriers, in which Co_3O_4 and Mn_2O_3 are respectively reduced to CoO and Mn_3O_4; and $CoAl_2O_4$ and Al_2O_3 perform as inert carrier. The kinetic analysis shows that the oxygen release of three oxygen carriers can be described by the nucleation and nuclei growth model. This means that after O_2 release the Cu-O bond (as an example) in the oxygen carrier is broken, generates Cu_2O active sites diffusing away from the reduction centers, and comes together to form Cu_2O clusters. The mechanism function $G(x)$, the activation energy and the pre-exponential factor have different expressions or different values for different oxygen carriers. The activation energies in the oxygen release of $CuO/CuAl_2O_4$, $Co_3O_4/CoAl_2O_4$ and Mn_2O_3/Al_2O_3 oxygen carriers, are 226.37, 130.06 and 65.90 kJ/mol respectively; and the pre-exponential factors are 2.99×10^6 s^{-1}, 4.96×10^3 s^{-1} and 27.37 s^{-1} respectively.

Keywords: kinetic mechanism; activation energy; chemical looping with oxygen uncoupling; oxy-fuel combustion; oxygen carrier

The oxy-combustion technology[1] for CO_2 capture has been paid increasing attention. The pure oxygen needed in oxy-combustion is normally obtained through cryogenic air separation technology, which results in higher costs of investment and operation. Another efficient CO_2 capture technology is chemical looping with oxygen uncoupling (CLOU)[2] with CO_2 capture efficiency higher than 95%[3]. It consists of air reactor (AR), fuel reactor (FR) and the oxygen carrier (OC) that cycles between AR and FR. OC releases gaseous oxygen in FR to provide an oxygen-existed atmosphere for fuel combustion, and uptakes oxygen from air for regeneration in the AR. Actually, OC which is capable of circularly uptaking/releasing oxygen in CLOU can also be used for oxygen preparation in oxy-combustion technology because the oxygen released by OC can replace the expensive oxygen from cryogenic air separation.

The oxygen preparation is critical for oxy-combustion and CLOU technologies. Thermodynamic analysis showed that CuO/Cu_2O, Co_3O_4/CoO and Mn_2O_3/Mn_3O_4 systems all have the ability to release oxygen[4], and exhibit great potential for oxygen preparation. Many researches have proved the performance of CuO, Co_3O_4 and Mn_2O_3 in terms of oxygen release. Leion et al[5,6] prepared CuO-based OC which is loaded on ZrO_2 through freeze granulation method. They found that the oxygen concentration in the reactor reached 10% because of the oxygen release from OC. Adánez-Rubio et al[7] and Gayán et al[8] prepared CuO-based OC which is loaded on ZrO_2, TiO_2, SiO_2, and Al_2O_3 with impregnation and mechanical mixing methods. They discovered that the oxygen concentration changed between 4–10% due to the release of oxygen from OC. The study of Arjmand et al[9] showed that CuO-based OC which is loaded on Al_2O_3 or $MgAl_2O_4$ both had the ability to release oxygen, the oxygen concentration varied between 0.5–2.5% with the temperature changing. Copper ore also displayed good performance of releasing oxygen. Wen et al[10] tested three kinds of copper ore. All of them showed a stable performance of releasing oxygen and the oxygen concentration changed between 2.0–3.5% under different temperatures. Li et al[11] tested the oxygen release performance of Co_3O_4-based OC loaded on Al_2O_3, and found that it still had good activity after long-term continuously uptaking/releasing oxygen cycles.

Received: 06-Aug-2012; Revised: 12-Oct-2012
* Corresponding author. E-mail; klinsmannzhb@163.com; Tel: 027-87545526-8208; Fax: 027-87545526.
Foundation item: Supported by the National Natural Science of China (50721005, 50936001) and the Program for New Century Excellent Talents in University (NCET-10-0395)

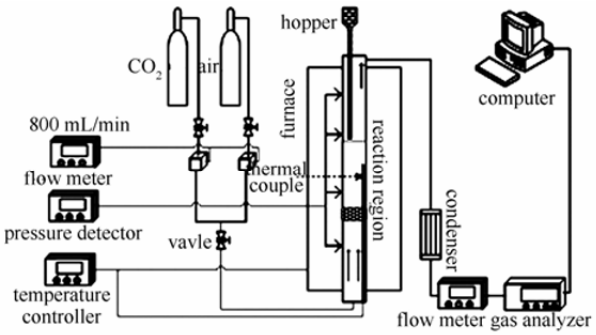

Fig. 1 An overview of the fluidized bed reactor system

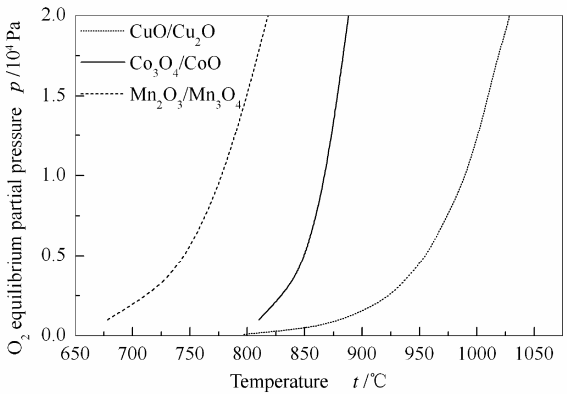

Fig. 2 Equilibrium partial pressure of O_2 under various temperatures for different oxygen carriers

Zhang et al[12] selected $Co_3O_4/CoAl_2O_4$ as OC, and prepared 20% oxygen-containing gas product in the parallel fixed bed reactor. Shulman et al[13] prepared Mn_2O_3 based OC, loaded on Fe_2O_3, NiO, and SiO_2, through freeze granulation method and the oxygen concentration was between 0.2%–2.5% in their fluidized bed experiments. Azimi et al[14] studied Mn_2O_3/Fe_2O_3 OC and found that the oxygen release performance was the best when the molar ratio of Mn and Fe was 2:1, which led to an oxygen concentration of 1% in the reaction tube. It was proven that the CuO, Co_3O_4 and Mn_2O_3 based OCs are potential to be used in CLOU and for pure oxygen preparation in oxy-combustion.

The rate of oxygen release is usually slower than that of oxygen uptaking, which is the main factor to determine the speed of CLOU and oxy-combustion. There are many factors in the oxygen release process, among which the reaction mechanism and activation energy are important to describe the difficulty of oxygen release. The reaction mechanism is helpful to understand the oxygen release process. Kinetic activation energy and pre-exponential factor can be used in numerical simulation for oxygen release process. These parameters have significant importance in deepening the understanding of CLOU and oxy-combustion. However, little attention has been paid to them in oxygen release process of OC in open references. Therefore, it is necessary to investigate the reaction mechanism and activation energy.

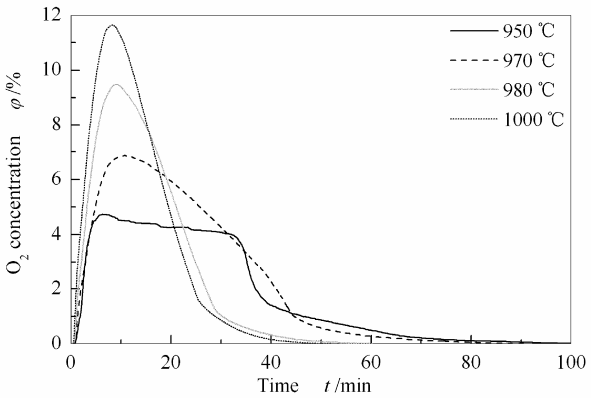

Fig. 3 Oxygen concentration profiles in the oxygen release for the $CuO/CuAl_2O_4$ under temperatures of 950, 970, 980 and 1000°C

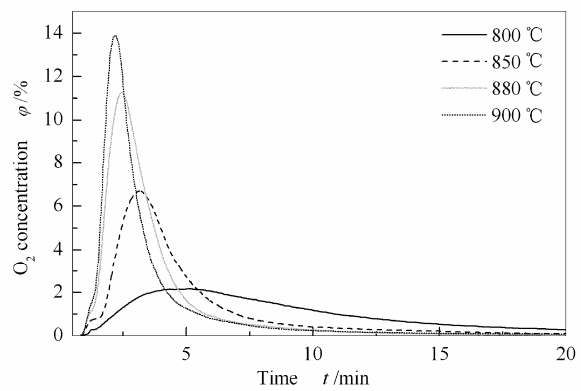

Fig. 4 Oxygen concentration profiles in the oxygen release for the $Co_3O_4/CoAl_2O_4$ under temperatures of 800, 850, 880 and 900°C

In this work, sol-gel-derived $CuO/CuAl_2O_4$, $Co_3O_4/CoAl_2O_4$ and Mn_2O_3/Al_2O_3 OCs were studied in a fluidized bed reactor, where the oxygen release characteristics under various temperatures were focused. Then, the reaction data under various temperatures were used to obtain the reaction mechanism, activation energy and pre-exponential factor for the three OCs through isothermal kinetics method.

1 OC preparation through sol-gel method

$CuO/CuAl_2O_4$, $Co_3O_4/CoAl_2O_4$ and Mn_2O_3/Al_2O_3 were prepared through the sol-gel method, and the mass fraction of CuO, Co_3O_4, and Mn_2O_3 is 60%. Sol-gel-derived OCs have good uniformity and mechanical strength which can improve their attrition resistance. The precursor of inert carrier is aluminum isopropoxide ($Al(C_3H_7O)_3$, KESHI Co., AR level, 99.9%) with 1 mol/L HNO_3 solution as sol agent for homogenization. The precursors of active component in the OCs are the corresponding metal nitrates, including $Cu(NO_3)_2{\cdot}3H_2O$ (Sinopharm Co., AR level, 99.9%), $Co(NO_3)_2{\cdot}3H_2O$ (Sinopharm Co., AR level, 99.9%), and $Mn(NO_3)_2$ solution (Sinopharm Co., 50% $Mn(NO_3)_2$ contained).

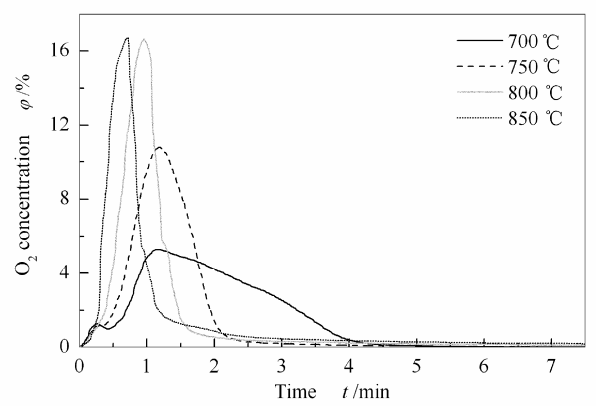

Fig. 5 Oxygen concentration profiles in the oxygen release for the Mn_2O_3/Al_2O_3 under temperatures of 700, 750, 800 and 850°C

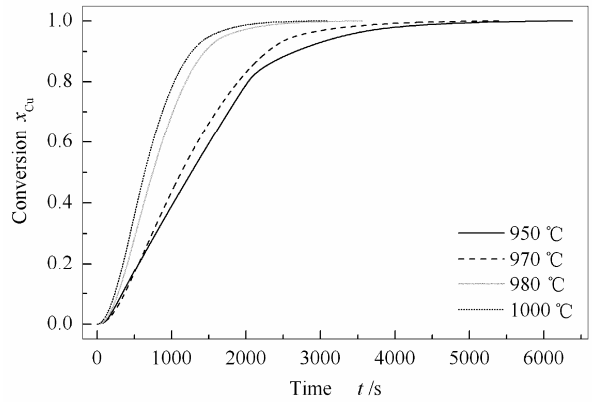

Fig. 6 $CuO/CuAl_2O_4$ conversion rate change as a function of time

According to the detailed steps for sol-gel method in references[15,16], we prepared the wet-gel with well-dispersed $Cu(NO_3)_2$, $Co(NO_3)_2$ and $Mn(NO_3)_2$. Then the wet-gel was put into an oven for drying under 80°C for 36 h, then under 100, 150, 200°C respectively for 5 h. After that, the dried-gel was placed into muffle furnace to calcine at 500°C for 6 h. For different active carriers, the samples were calcined at different temperatures for 6–10 h. The calcining temperatures of CuO, Co_3O_4, and Mn_2O_3 based OC are 1000, 800 and 900°C, respectively. After calcination, block products can be obtained, which was then ground and screened after cooling down. Particles in the size range of 0.125–0.180 mm were used as OC in the experiments.

2 Phase composition analysis

The phase composition of the fresh and the used OC particles were characterized by SHIMADZU XRD-7000 instrument with Cu rake under 2θ=10–90°. The maximum tube voltage and current are 40 kV and 30 mA. The results illustrate that CuO based OC is composed of two crystalline phases, CuO and $CuAl_2O_4$, however, no Al_2O_3 was observed. This means that all Al_2O_3 reacted completely with CuO in the OC to form $CuAl_2O_4$ in the calcining process. Co_3O_4-based OC is made up of Co_3O_4 and $CoAl_2O_4$ which is generated through Co_3O_4 reacting with Al_2O_3 in calcining process. Just like CuO-based OC, Al_2O_3 also has been completely transformed into $CoAl_2O_4$. In fresh Mn_2O_3 based OC, Mn_2O_3 and Al_2O_3 show the main phases.

3 Fluidized bed system

The tests of oxygen release characteristics of OCs were conducted under atmosphere pressure in a laboratory scale fluidized bed reactor as shown in Figure 1. A straight stainless steel tube (i.d.=26 mm, length=892 mm) is located inside the furnace.

A porous plate whose pore diameter is smaller than 0.125 mm to prevent OC particles leaking out is located at 400 mm from the bottom of the reaction tube. The temperature inside the reaction tube is monitored by K-thermocouple in time. Oxygen release is tested under highly pure CO_2 atmosphere, which was followed by the regeneration in air atmosphere. 800 mL/min CO_2 and air were flowed into the reactor through the porous plate. The mass of $CuO/CuAl_2O_4$ based OC is 40 g, and that of $Co_3O_4/CoAl_2O_4$ and Mn_2O_3/Al_2O_3 based OCs is both 30 g. Before test CO_2 was introduced into the reaction tube to sweep the residual O_2. Then the reactor was heated to 700–1000°C in CO_2 atmosphere. As the temperature was stable for 30 min, the OC particles was added quickly into the reactor. The start and completion of the oxygen release were respectively marked by the emergence and vanishing of oxygen in the gas products. After the oxygen release finished, the reactor was cooled down to 600–1000°C. When the temperature was stable for 30 min, the fluidized gas was switched to air for OC oxidization. When the O_2 concentration reached 20.95%, it was considered that the OC oxidization is complete. The tail gas stream was first introduced into an electric condenser to remove the water steam, and then into the gas analyzer to detect the components.

4 Oxygen release characteristics

4.1 Equilibrium partial pressure of O_2

The equilibrium partial pressures of O_2 under various temperatures for CuO/Cu_2O, Co_3O_4/CoO and Mn_2O_3/Mn_3O_4 systems are shown in Figure 2 which reflects the maximum O_2 concentration when OC releases O_2. Oxygen will release when the oxygen partial is lower than the equilibrium value, while the OC will uptake oxygen from the environment when the pressure is higher than the equilibrium curve. Mn_2O_3 releases oxygen obviously when the temperature is between 700–850°C, and the corresponding equilibrium partial pressure of O_2 changes between 2.5×10^3–5.00×10^4 Pa.

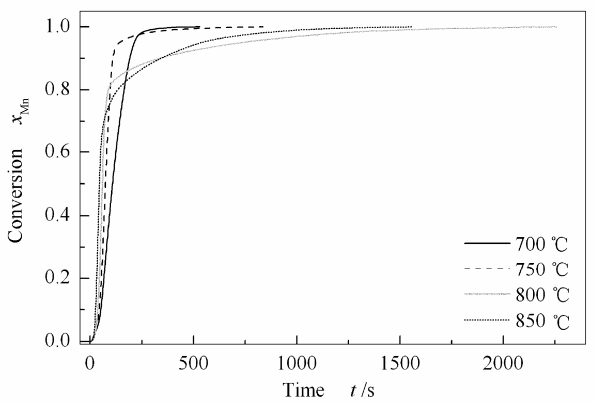

Fig. 7 Mn_2O_3/Al_2O_3 conversion rate change as a function of time

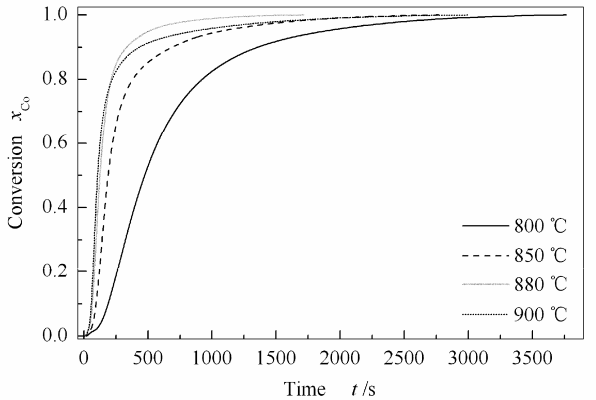

Fig. 8 $Co_3O_4/CoAl_2O_4$ conversion rate change as a function of time

However, the evident oxygen release from CuO and Co_3O_4 starts when the temperature is above 900 and 800°C respectively. It is obvious that higher temperature is beneficial for the release of active oxygen in these OCs. However, a lower temperature should be taken into consideration to prevent possible agglomeration of OC particles. In addition, CLOU is usually based on circulating fluidized bed reactor with the operating temperature always below 1000°C. Therefore, the oxygen release temperatures of $CuO/CuAl_2O_4$, $Co_3O_4/CoAl_2O_4$ and Mn_2O_3/Al_2O_3 were selected between 700–1000°C.

4.2 Oxygen releasing experiment in fluidized bed

Oxygen carrier can release gaseous oxygen under CO_2 atmosphere because the O_2 concentration is zero which is far below the equilibrium partial pressure of O_2. In order to study the oxygen release kinetic characteristics, the oxygen release experiments of three OCs in four different temperatures were carried out. The oxygen releasing temperatures for $CuO/CuAl_2O_4$ OC were 950, 970, 980 and 1000°C; for $Co_3O_4/CoAl_2O_4$ OC were 800, 850, 880 and 900°C; and for Mn_2O_3/Al_2O_3 were 700, 750, 800 and 850°C.

4.2.1 oxygen release of $CuO/CuAl_2O_4$

Table 1 Part of the generally used 40 mechanism functions

Reaction Model	$G(x)$	
Jander function	$[1-(1-x)^{1/2}]^n$	(n=1/2, 2)
Z-L-T function	$[(1+x)^{-1/3}-1]^2$	
Avrami-Erofeev	$[-\ln(1-x)]^n$	(n=1/4, 1/3, 2/5, 1/2, 2/3, 3/4, 1, 3/2, 2, 3, 4)
P-T function	$\ln[(1-x)/x]$	
Mampel	x^n	(n=1/4, 1/3, 1/2, 1, 3/2, 2)
	$1-(1-x)^n$	(n=1/4, 1/3, 1/2, 2, 3, 4)
	$(1-x)^{-n}$	(n=1, 1/2)
Index law	$\ln x^n$	(n=1, 2)

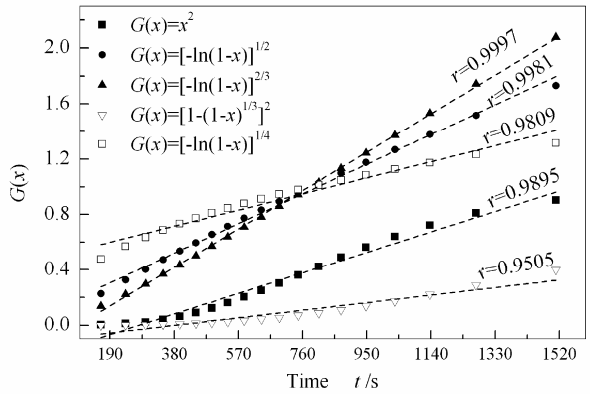

Fig. 9 Linearity of different $G(x)$ and t under 1000°C for $CuO/CuAl_2O_4$ oxygen carrier

As the temperature was between 950–1000°C, the oxygen release process of $CuO/CuAl_2O_4$ OC is shown in Figure 3. The maximum O_2 concentration is about 5% at 950°C. As the temperature increasing, the O_2 concentration reaches 7% at 970°C, 9.5% at 980°C, and 12% at 1000°C, meanwhile the period of oxygen release decreases from 80 min at 950°C to 50 min at 1000°C. This suggests that the increasing temperature can promote the oxygen release of CuO-based OC. In addition, CuO-based OCs still have good reactivity after repeatedly uptaking and releasing oxygen and the agglomeration phenomenon does not appear. The XRD test of the completely reduced OC showed that the CuO-based OC is composed of Cu_2O, $CuAlO_2$ and Al_2O_3, demonstrating that CuO and $CuAl_2O_4$ involve in the oxygen release as active phases.

4.2.2 Oxygen release of $Co_3O_4/CoAl_2O_4$

The oxygen release process of $Co_3O_4/CoAl_2O_4$ at 800–900°C is shown in Figure 4. The releasing rate is very slow at 800°C, and the maximum oxygen concentration is just about 2%. The O_2 concentration changes between 2%–14%, and the reaction time changes between 15–20 min depending on the temperature. The OC possesses a relatively good reactivity in the repeated oxygen uptake/release with no obvious agglomeration.

Table 2 Related coefficients of $G(x)$ and t under various temperatures and different mechanism functions for $CuO/CuAl_2O_4$ oxygen carrier

$G(x)$	Temperature t/°C			
	950	970	980	1000
x^2	0.9845	0.9922	0.9894	0.9895
$[-\ln(1-x)]^{1/4}$	0.9762	0.9839	0.9836	0.9809
$[-\ln(1-x)]^{1/2}$	0.9953	0.9987	0.9989	0.9981
$[-\ln(1-x)]^{2/3}$	0.9982	0.9986	0.9992	0.9997
$[1-(1-x)^{1/3}]^2$	0.9536	0.9412	0.9451	0.9505

The XRD tests showed that Co_3O_4 was reduced to CoO, and $CoAl_2O_4$ did not change after oxygen release. This indicates that $CoAl_2O_4$ is an inert phase in the oxygen release process. The difference from $CuO/CuAl_2O_4$ is that the time of oxygen release was significantly shortened, and the peak of O_2 concentration was higher than that of $CuO/CuAl_2O_4$. This phenomenon is related to the amount and the kinetic characteristics of the OC. A smaller amount of $CoO/CoAl_2O_4$ led to shorter reaction time. The subsequent kinetic analysis shows that the activation energy of $Co_3O_4/CoAl_2O_4$ is lower than that of $CuO/CuAl_2O_4$, so Co_3O_4-based OC is easier and faster in oxygen release than CuO-based OC. What is more, it is noted that $CuAl_2O_4$ in $CuO/CuAl_2O_4$ can also release oxygen, which resulted in more oxygen releasing. Hence, the oxygen release time of $CuO/CuAl_2O_4$ is extended.

4.2.3 Oxygen release of Mn_2O_3/Al_2O_3

Compared with CuO and Co_3O_4 based OCs, the oxygen release temperature of Mn_2O_3 based OC is much lower. It starts to release oxygen at 700°C with oxygen concentration peak of 5%, as shown in Figure 5. As the temperature rises to 750 and 800°C, the oxygen concentration peak reaches 11% and 16% respectively. When the temperature increases to 850°C, the oxygen concentration has no apparent increase, but the oxygen release time decreases. The XRD results manifested that Mn_2O_3 was reduced to Mn_3O_4, and Al_2O_3 did not change after oxygen release. The later kinetic analysis shows that the activation energy of Mn_2O_3/Al_2O_3 is lower than that of $CuO/CuAl_2O_4$ and $Co_3O_4/CoAl_2O_4$ in oxygen release process, which leads to faster and easier oxygen release from Mn_2O_3/Al_2O_3. Besides, a smaller amount of Mn_2O_3/Al_2O_3 used results in fewer amounts of gaseous oxygen. The oxygen releasing time of Mn_2O_3/Al_2O_3 is about 4–5 min, which is just a quarter of that of the same amount of Co_3O_4 based OC.

5 Kinetic mechanism of oxygen release

In order to further explore the kinetic characteristics of OCs, the conversion rate x of OCs at different temperatures were calculated by Eq. 1. The conversion rates of $CuO/CuAl_2O_4$, $Co_3O_4/CoAl_2O_4$ and Mn_2O_3/Al_2O_3 are represented by x_{Cu}, x_{Co}, x_{Mn} respectively. The relation between conversion rate of OCs and reaction time is shown in Figures 6–8.

$$x = \frac{\int_0^t \varphi_{O_2} Q_{out} \mathrm{d}t}{\int_0^{t,ad} \varphi_{O_2} Q_{out} \mathrm{d}t} \tag{1}$$

In Eq. 1, Q_{out} (mol/s) is the molar flow of gas products, φ_{O_2} (mol%) is molar concentration of O_2 in the gas products, and t_{red} (s) is the end time of oxygen release.

Table 3 Intercepts of the fitting lines under different $G(x)$ and temperatures of $CuO/CuAl_2O_4$ oxygen carrier

$G(x)$	Temperature t/°C				AVG	SD (σ)
	950	970	980	1000		
$[-\ln(1-x)]^{1/2}$	0.19144	0.13016	0.07058	0.09080	0.100	0.068
$[-\ln(1-x)]^{2/3}$	–0.0086	–0.008497	–0.16251	–0.13760	–0.098	0.059

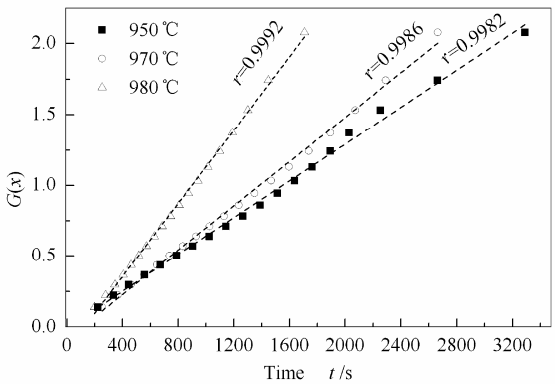

Fig. 10 Linearity of $G(x)=[-\ln(1-x)]^{2/3}$ and t under various temperatures for $CuO/CuAl_2O_4$ oxygen carrier

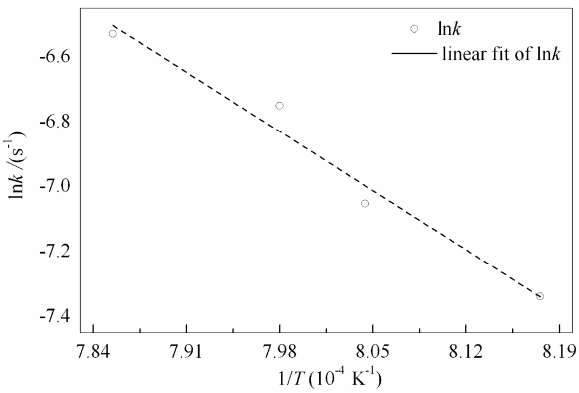

Fig. 11 Linearity of ln$k$ and 1/T for CuO based oxygen carrier

Table 4 Related coefficients of $G(x)$ and t under various temperatures and different mechanism functions ($Co_3O_4/CoAl_2O_4$ oxygen carrier)

$G(x)$	Temperature t/°C			
	800	850	880	900
x^2	0.9925	0.9518	0.9536	0.9351
$[-\ln(1-x)]^{1/2}$	0.9931	0.9488	0.9548	0.9311
$[-\ln(1-x)]^{2/3}$	0.9992	0.9695	0.9735	0.9553
$[-\ln(1-x)]^{3/4}$	0.9997	0.9774	0.9804	0.9649
$-\ln(1-x)$	0.9932	0.9925	0.9929	0.9851
$1-(1-x)^{1/4}$	0.9995	0.9755	0.9778	0.9625
$1-(1-x)^{1/3}$	0.9992	0.9679	0.9709	0.9533

Reaction kinetics always focuses on activation energy E (kJ/mol), pre-exponential factor A (s^{-1}), kinetic constant k, the integrated form of mechanism function $G(x)$ or the differential form $f(x)$. The relationship between E, A and k can be expressed by Arrhenius formula (Eq. 2). Mechanism function $f(x)$ and k can mutually convert through Eq. 3, and the relationship between $f(x)$ and $G(x)$ is described by Eq. 4. Equation 5 is obtained through combining Eqs. 2–4. In Eq. 5, k is constant at constant temperature and $G(x)$ is linearly related to t, which is used to determine the mechanism function $G(x)$ of the reaction process. The linear correlation between $G(x)$ and t is described by coefficient r. When r is closer to 1, the linearity is better. And the corresponding $G(x)$ is more possibly the mechanism function that we seek. We calculated the coefficient r by bringing 40 $G(x)$ functions[17] (shown in Table 1) into Eq. 5, which resulted in many $G(x)$s that exhibit good linear correlation with t. Therefore, the intercept of the line formed by G(x) and t was further calculated to determine the mechanism function. The $G(x)$ with intercept near to zero was chosen as the mechanism function of this reaction. The kinetic constant k at various temperatures was calculated by Eq. 5. By putting k and temperature T into Eq. 6, E and A were obtained through the linear relationship of ln$k$ and 1/T.

$$k = A\exp(-\frac{E}{RT}) \tag{2}$$

$$\frac{\mathrm{d}x}{\mathrm{d}t} = k(T)f(x) \tag{3}$$

$$G(x) = \int_0^t \frac{1}{f(x)}\mathrm{d}x \tag{4}$$

$$G(x) = \int_0^t A\exp(-\frac{E}{RT})\mathrm{d}t = kt \tag{5}$$

$$\ln k = -\frac{E}{RT} + \ln A \tag{6}$$

Figure 9 shows the linearity of different $G(x)$s and t for $CuO/CuAl_2O_4$ at 1000°C when r is close to 1. The coefficient r of $G(x)$ and t was obtained by putting (x_{Cu}, t) at various temperatures into these mechanism functions, as listed in Table 2. When the mechanism functions are $G(x)=[-\ln(1-x)]^{1/2}$ and $G(x)=[-\ln(1-x)]^{2/3}$, the values of r are both larger than 0.99 and have little difference with each other.

To further recognize the probable $G(x)$, the intercepts were calculated by linear fitting ($G(x)$, t), and the results are given in Table 3. When $G(x)=[-\ln(1-x)]^{2/3}$, the absolute value of corresponding intercepts and standard deviations are the smallest. This shows that the intercepts of the fitting line are almost near zero. Furthermore, the (x_{Cu}, t) data at various temperatures was used in $G(x)=[-\ln(1-x)]^{2/3}$ to calculate the corresponding coefficient r. The linear relation of $G(x)$ and t under various temperatures is presented in Figure 10, in which all the corresponding coefficients are larger than 0.998. Therefore, the oxygen release process of $CuO/CuAl_2O_4$ can be described by the mechanism function $G(x)=[-\ln(1-x)]^{2/3}$, which belongs to the nucleation and nuclei growth model. That is, after O_2 releases, the Cu-O bond in the OC is broken, generates Cu_2O active site, and then diffuses away from the reduction centers and comes together to form Cu_2O clusters. The Cu_2O clusters produced from the separate phase of CuO in the $CuO/CuAl_2O_4$ oxygen carrier grow bigger to form Cu_2O phase. The Cu_2O clusters produced from the crystalline phase of $CuAl_2O_4$ combine with the Al_2O_3 phase in the crystalline themselves, and then grow bigger to form $CuAlO_2$ phase.

The linearity of ln$k$ and 1/T, when the mechanism function was $G(x)=[-\ln(1-x)]^{2/3}$, is shown in Figure 11. The slope and Y intercept of the line can be calculated by linearly fitting the four experimental data in Figure 11, and then the activation energy E of 226.37 kJ/mol and pre-exponential factor A of 2.99×10^6 s^{-1} are obtained. For the $Co_3O_4/CoAl_2O_4$ OC, when bringing the data (x_{Co}, t) at 800°C into the 40 mechanism functions, many $G(x)$s making r close to 1 were found, as listed in Table 4. By comparing with each other, we found that when $G(x)=[-\ln(1-x)]^{3/4}$ and $G(x)=-\ln(1-x)$, the values of r are larger than others at various temperatures. The intercepts of the fitting lines are shown in Table 5, in which the average values of intercepts most approximates to zero and the standard deviation is the smallest when the mechanism function is $G(x)=[-\ln(1-x)]^{3/4}$.

Table 5 Intercepts of the fitting lines under different $G(x)$ and temperatures for $Co_3O_4/CoAl_2O_4$ oxygen carrier

$G(x)$	Temperature t/°C				AVG	SD (σ)
	800	850	880	900		
$[-\ln(1-x)]^{3/4}$	-0.2245	-0.0810	-0.1781	-0.0487	-0.133	0.071
$-\ln(1-x)$	-0.5535	-0.3901	-0.5190	-0.3528	-0.454	0.084

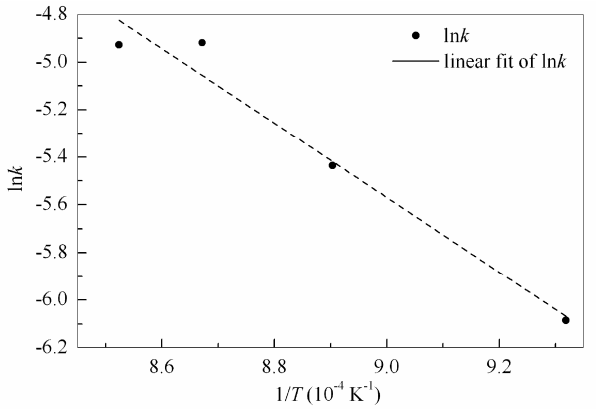

Fig. 12 Linearity of ln$k$ and 1/T for Co_3O_4 based oxygen carrier

Table 6 Related coefficients of $G(x)$ and t under various temperatures and different mechanism functions

$G(x)$	Temperature t/°C			
	700	750	800	850
$[-\ln(1-x)]^{2/5}$	0.9978	0.9843	0.9920	0.9522
$[-\ln(1-x)]^{1/2}$	0.9994	0.9873	0.9927	0.9637
$[-\ln(1-x)]^{2/3}$	0.9961	0.9876	0.9895	0.9775
$1-(1-x)^{1/2}$	0.9985	0.9785	0.9833	0.9597

Therefore, $G(x)=[-\ln(1-x)]^{3/4}$ can be used to describe the oxygen release process of $Co_3O_4/CoAl_2O_4$. Similar to the CuO-based OC, the oxygen release of $Co_3O_4/CoAl_2O_4$ can also be described by the nucleation and nuclei growth model.

The linearity of ln$k$ and 1/T under the mechanism function $G(x)=[-\ln(1-x)]^{3/4}$ is shown in Figure 12. Through Eq. 6 the activation energy E and pre-exponential factor A of oxygen release are 130.06 kJ/mol and 4.96×10^3 s^{-1}, respectively.

For Mn_2O_3/Al_2O_3, when bringing the data (x_{Mn}, t) under 700°C into four $G(x)$s in Table 6, the coefficient r values are larger than the others. At various temperatures the best linearity of $G(x)$ and t emerge when $G(x)=[-\ln(1-x)]^{2/5}$ and $G(x)=[-\ln(1-x)]^{1/2}$ were used as mechanism functions. For $G(x)=[-\ln(1-x)]^{2/5}$, the intercept and standard deviation of the G(x)-t fitting line are –0.0743 and 0.165, respectively, which are the smallest among three mechanism functions. Therefore, the most probable mechanism function in the oxygen release for Mn_2O_3/Al_2O_3 was confirmed as $G(x)=[-\ln(1-x)]^{2/5}$. Similar to $CuO/CuAl_2O_4$ and $Co_3O_4/CoAl_2O_4$, the oxygen release process for Mn_2O_3/Al_2O_3 can also be described by the nucleation and nuclei growth model. Then, the activation energy E and pre-exponential factor A in oxygen release were determined as 65.90 kJ/mol and 27.37 s^{-1} respectively.

Table 7 Intercepts of the fitting lines under different $G(x)$ and temperatures

$G(x)$	Temperature t/°C				AVG	SD (σ)
	700	750	800	850		
$[-\ln(1-x)]^{2/5}$	0.0942	-0.1198	0.3241	0.0526	-0.0743	0.165
$[-\ln(1-x)]^{1/2}$	-0.0816	-0.3431	-0.5881	-0.1425	-0.2889	0.198
$[-\ln(1-x)]^{2/3}$	-0.3547	-0.6970	-1.0067	-0.4563	-0.6287	0.251

6 Conclusions

The $CuO/CuAl_2O_4$, $Co_3O_4/CoAl_2O_4$ and Mn_2O_3/Al_2O_3 OCs can release oxygen in CO_2 atmosphere. The phase compositions of these OCs change after oxygen release. The phases of CuO and $CuAl_2O_4$ in CuO-based OC perform as active components in the oxygen release, which are decomposed to Cu_2O, $CuAlO_2$ and Al_2O_3 with gaseous O_2 generation. However, the phase of Al_2O_3 in MnO-based OC and that of $CoAl_2O_4$ in Co_3O_4-based OC perform as inert carriers. Only Co_3O_4 and Mn_2O_3 can release oxygen in $Co_3O_4/CoAl_2O_4$ and Mn_2O_3/Al_2O_3 oxygen carriers, and are respectively reduced to CoO and Mn_3O_4.

The isothermal kinetics analysis shows that the mechanism functions $G(x)$, the activation energies and the pre-exponential factor are different for various oxygen carriers. For $CuO/CuAl_2O_4$, $Co_3O_4/CoAl_2O_4$ and Mn_2O_3/Al_2O_3 oxygen carrier, the mechanism functions are $G(x)=[-\ln(1-x)]^{2/3}$, $G(x)=[-\ln(1-x)]^{3/4}$ and $G(x)=[-\ln(1-x)]^{2/5}$, respectively. The activation energies are 226.37 kJ/mol, 130.06 kJ/mol and 65.90 kJ/mol; and the pre-exponential factors are 2.99×10^6 s^{-1}, 4.96×10^3 s^{-1} and 27.37 s^{-1} respectively. Comparison of the activation energies suggests that Mn_2O_3-based OC is the easiest to release oxygen, and CuO-based OC is the most difficult, and Co_3O_4 base OC is medium.

The oxygen release of the three oxygen carriers can be described by the nucleation and nuclei growth model. The change processes of internal structure of the OCs and the composition change can be described by chemical nucleation and physical nuclei growth in the oxygen-releasing process.

References

[1] Xiong J, Zhao H, Zheng C, Liu Z, Zeng L, Liu H, Qiu J. An economic feasibility study of O_2/CO_2 recycle combustion technology based on existing coal-fired power plants in China. Fuel, 2009, 88(6): 1135–1142.

[2] Lyngfelt A, Mattissopn T. Trestegsförbränning för avskiljning av koldioxid. Sweden, 2005.

[3] Abad A, Adánez-Rubio I, Gayán P, García-Labiano F, Diego L F, Adánez J. Demonstration of chemical-looping with oxygen uncoupling (CLOU) process in a 1.5 kW_{th} continuously

operating unit using a Cu-based oxygen-carrier. Int J of Greenh Gas Con, 2012, 6(1): 189–200.

[4] Mattissopn T, Lyngfelt A, Leion H. Chemical-looping with oxygen uncoupling for combustion of solid fuels. Int J Greenh Gas Con, 2009, 3(1): 11–19.

[5] Leion H, Mattissopn T, Lyngfelt A. Using chemical-looping with oxygen uncoupling (CLOU) for combustion of six different solid fuels. Energy Procedia, 2009, 1(1): 447–453.

[6] Leion H, Mattissopn T, Lyngfelt A. Chemical looping combustion of solid fuels in a laboratory fluidized-bed reactor. Oil Gas Sci Technol Rev IFP Energies nouvelles, 2011, 66(2): 201–208.

[7] Adánez-Rubio I, Gayán P, García-Labiano F, Diego L F, Adánez J, Abad A. Development of CuO-based oxygen-carrier materials suitable for chemical-looping with oxygen uncoupling (CLOU) process. Energy Procedia, 2011, 4(1): 417–424.

[8] Gayán P, Adánez-Rubio I, Abad A, Diego L F, García-Labiano F, Adánez J. Development of Cu-based oxygen carriers for chemical-looping with oxygen uncoupling (CLOU) process. Fuel, 2012, 96(1): 226–238.

[9] Arjmand M, Azad A, Leion H, Lyngfelt A, Mattisson T. Prospects of Al_2O_3 and $MgAl_2O_4$-supported CuO oxygen carriers in chemical-looping combustion (CLC) and chemical-looping with oxygen uncoupling (CLOU). Energy Fuels, 2011, 25(11): 5493–5502.

[10] Wen Y, Li Z, Xu L, Cai N. Experimental study of natural cuore particles as oxygen carriers in chemical looping with oxygen uncoupling (CLOU). Energy Fuels, 2012, 26(6): 3919–3927.

[11] Li Z, Zhang T, Cai N. Experimental study of O_2−CO_2 production for the oxyfuel combustion using a co-based oxygen carrier. Ind Eng Chem Res, 2008, 47(19): 7147–7153.

[12] Zhang T, Li Z, Cai N. Continuous O_2-CO_2 production using a Co-based oxygen carrier in two parallel fixed-bed reactors. Korean J Chem Eng, 2009, 26(3): 845–849.

[13] Shuiman A, Cleverstam E, Mattisson T, Lyngfelt A. Manganese/Iron, Manganese/Nickel, and Manganese/Silicon oxides used in chemical-looping with oxygen uncoupling (CLOU) for combustion of methane. Energy Fuels, 2009, 23(10): 5269–5275.

[14] Azimi G, Leion H, Mattisson T, Lyngfelt A. Chemical-looping with oxygen uncoupling using combined Mn-Fe oxides, testing in batch fluidized bed. Energy Procedia, 2011, 4(1): 370–377.

[15] Mei D F, Zhao H B, Ma Z J, Zheng C G. Preparation method study on Fe_2O_3/Al_2O_3 oxygen carrier. Journal of Fuel Chemistry and Technology, 2012, 40(7): 795–802.

[16] Zhao H B, Liu L M, Xu D, Zheng C G, Liu G J, Jiang L L. $NiO/NiAl_2O_4$ oxygen carriers prepared by sol-gel for chemical-looping combustion fueled by gas. Journal of Fuel Chemistry and Technology, 2008, 36(3): 261–266.

[17] Hu R Z, Gao S L, Zhao F Q, Shi Q Z, Zhang T L, Zhang J J. Thermal analysis kinetics. Beijing: Science Press, 2008: 127–131.